Inhomogeneous broadening of optical transitions dominated by low-symmetry crystal-field components in Cr^{3+}-doped gallogermanates

Marek Grinberg
Institute of Physics, Nicolaus Copernicus University, Grudziadzka 5/7, 87-100 Torun, Poland

Peter I. Macfarlane, Brian Henderson, and Keith Holliday
Department of Physics and Applied Physics, University of Strathclyde, Glasgow G4 0NG, United Kingdom
(Received 6 April 1995)

The optical spectroscopy of strong- and weak-field sites of Cr^{3+}-doped gallogermanates have been investigated using fluorescence line narrowing, selective excitation, and selective fluorescence lifetime measurements. A statistical model has been used to model the spectroscopic data obtained from the R-line fluorescence of the strong-field sites whilst an adiabatic model of the spin-orbit and electron-phonon coupling interactions has been used to model the broadband absorption and emission of the weak-field sites. For both strong- and weak-field sites it is shown that inhomogeneous broadening is dominated by the nonoctahedral component of the crystal field rather than by variation of the octahedral crystal-field strength.

INTRODUCTION

The inhomogeneous broadening of optical transitions in solids is of great importance to the fundamental understanding of the interaction between optically active impurity ions and their host lattices. The ability to predict the nature and magnitude of inhomogeneous broadening in crystals provides information vital for "crystal-field engineering," a term that refers to the production of optical materials that conform to a set of predetermined optimized characteristics. The widths of spectral features are of particular importance for gain media used in tuneable and short pulse lasers and for spectral hole-burning materials.

Purely electronic transitions in perfect crystals have linewidths determined entirely by lifetime and dephasing mechanisms. The dominant contribution to dephasing comes from electron-phonon interactions resulting in a homogeneous linewidth that is highly temperature dependent. In a real crystal the local environment of different impurity ions in crystallographically equivalent sites varies by small, random amounts. The resulting superposition of homogeneous line shapes produces a broadened, nominally Gaussian inhomogeneous line shape. Normally, the inhomogeneous contribution to broadening is only weakly temperature dependent and so homogeneous broadening usually dominates the linewidth above a certain temperature (the broadening crossover temperature). For most materials this is below room temperature.

It is, however, possible to engineer a substantial increase in the magnitude of inhomogeneous broadening. This is most vividly illustrated by glassy hosts in which crystalline periodicity is lacking and, despite the usual accompanying increase in homogeneous linewidths, the randomly disordered impurity sites lead to line shapes dominated by inhomogeneous broadening even at room temperature. However, there are ways in which the broadening crossover temperature may be increased without forfeiting the crystalline nature of the material. Substitutional disorder in crystals occurs when two or more constituent ions have interchangeable lattice positions. While the stoichiometry and periodicity of the crystal is maintained, the local environment varies throughout the structure. Optically active impurity ions experience different crystal fields as a result of this local variation. The inhomogeneous broadening of the zero-phonon electronic transitions of the impurity ions are consequently significantly broadened such that other sources of inhomogeneous broadening are negligible in comparison. Other spectral features are similarly broadened.

Inhomogeneous broadening through substitutional disorder is strongest when it is the nearest-neighbor ions that are randomly occupied. For instance, the $^7F_0 \rightarrow {}^5D_0$ transition of Sm^{2+} in BaFCl is broadened from less than 2 cm^{-1} to more than 50 cm^{-1} at low temperatures through the addition of bromine to the melt to produce $BaFCl_xBr_{1-x}$.[1] Such is the magnitude of the effect that inhomogeneous broadening dominates homogeneous broadening up to temperatures in excess of 300 K. This discovery prompted a successful search for room-temperature persistent spectral hole-burning materials.[2]

The sharp line spectra of Cr^{3+} ions have been used as probes of disorder in both crystalline and glassy solids. In dilute ruby (i.e., Cr^{3+} in Al_2O_3) the $^2E \rightarrow {}^4A_2$ luminescence lines (R lines) are typically narrower than 1 cm^{-1}.[3] For these R lines, the effect of even second-nearest-neighbor substitutional disorder can be considerable. In the case of some Cr^{3+}-doped oxides (e.g., the garnets and gallogermanates), it is supposed that the randomly occupied second-nearest neighbors affect the separation and position of nearest-neighbor oxygen ions. For instance, in $Gd_3Sc_2Ga_3O_{12}$ the R lines are broadened to 12 cm^{-1},[4] and by about twice that amount in $Ca_3Ga_2Ge_4O_{14}$

(CGGO) and $Sr_3Ga_2Ge_4O_{14}$ (SGGO).[5] In contrast, the R line in glassy hosts may have half widths as large as $\sim 200\ cm^{-1}$.[6,7]

Of particular interest in the cases of CGGO and SGGO is the fact that the R lines are accompanied by broadband emission from centers radiating through the ${}^4T_2 \rightarrow {}^4A_2$ transition. This suggests that there are either crystallographically inequivalent sets of sites for Cr^{3+} in these materials or that the random occupation of Ga and Ge sites is sufficient to produce a distribution of crystal-field strengths at a single crystallographic site such that the lowest excited state may be either ${}^4T_2$ or ${}^2E$ for Cr^{3+}. Multiple separated R lines have been observed in several materials such as yttrium aluminum garnet[8] and ascribed to substitutional disorder and so either explanation is feasible on the basis of optical spectroscopy alone. There is strong evidence from electron paramagnetic resonance (EPR) studies that two inequivalent sites do exist in the gallogermanates.[9] Both sites have strong trigonal distortions along the c axis, the distinction between sites being a small off-axis distortion resulting in orthorhombic symmetry in one case.

For the purposes of this paper, a strong crystal field is defined as resulting in the ${}^2E$ state being lower than the ${}^4T_2$ state and vice versa for weak crystal fields. In strong-field sites at low temperature the luminescence of Cr^{3+} ions is predominantly via the R lines, whereas in weak-field sites the broadband ${}^4T_2 \rightarrow {}^4A_2$ transition is dominant. It should be noted that the difference in crystal-field strength between weak- and strong-field sites may actually be very small, the distinction is between two sets of ions experiencing an intermediate crystal field close to the crossing between ${}^4T_2$ and ${}^2E$ states.[10,11]

This paper reports an experimental and theoretical investigation of inhomogeneous broadening in CGGO:Cr^{3+} and SGGO:Cr^{3+}, materials that have been suggested as laser gain media.[12] The results of excitation spectroscopy, resonant and nonresonant fluorescence lifetime measurements and high- and low-resolution fluorescence line narrowing (FLN) experiments are used to provide parameters to fit to an adiabatic model.[13] Although these materials have subsequently been shown to be unsuitable for real applications in lasers,[5] the methods of investigation and calculation described here are of general applicability.

EXPERIMENTAL DETAILS

Experiments were conducted on high-quality samples of SGGO and CGGO of dimension $6 \times 3 \times 3\ mm^3$ doped with 0.5 at. % chromium as described previously.[5] They were cooled to 14 K by attachment to the cold finger of a cryorefrigerator.

Luminescence spectra in the range 6900–14 500 cm^{-1} were excited by either a dye laser operating with rhodamine 6 G, a pulsed dye laser operating with DCM or a single frequency Ti:sapphire ring laser. Emitted light was dispersed in a 0.5 m grating monochromator and detected by a nitrogen-cooled germanium detector with lock-in amplification.

Fluorescence line narrowing studies used the highly monochromatic output of the Ti:sapphire laser tuned to excite the R lines resonantly. The jitter-limited linewidth of the laser emission is thought to have been well below 1 MHz even though active stabilization was not employed: the long-term drift of the output was substantially greater than this. Nevertheless, the detection resolution of all experimental arrangements dwarfed the effective laser linewidth. The wavelength of excitation was recorded by a wave meter. Emission was dispersed in a 1 m monochromator and detected by a cooled photomultiplier tube connected to a photon counter. Luminescence was isolated from laser scatter by chopping the laser and gating the photon counter. Higher-resolution fluorescence line narrowing spectra were recorded by analyzing the emission using a Fabry-Pérot étalon set with its plates 0.5 mm apart to give a free spectral range of 5 cm^{-1} and an effective resolution of 0.2 cm^{-1}.

Lifetimes of the resonantly excited and detected R lines were obtained using the boxcar integration technique by scanning the delay of the photon counter gate from 0.1 to 1.5 ms after excitation. Resonant fluorescence was selected using the 1 m monochromator. Lifetimes of the broadband emission were measured by exciting the sample at 17 200 cm^{-1} using a rhodamine 6 G dye cell pumped by a pulsed nitrogen laser. The resulting luminescence decay was detected for the following 50 μs by a photomultiplier tube and averaged by a digital oscilloscope.

EXPERIMENTAL RESULTS

A comprehensive series of fluorescence spectra were recorded for both materials using excitation energies between 17 500 and 13 300 cm^{-1}. Representative spectra have been published previously[5] but slightly modified spectra are presented in Fig. 1 for which the response of the detection apparatus has been taken into account. The main features are a sharp R-line feature at about 14 500 cm^{-1} and a broadband that stretches from about 7140 cm^{-1} to about 13 300 cm^{-1}. These features correspond to the ions that experience strong and weak crystal fields, respectively. Of importance to this investigation is the position of the peak of the broadband fluorescence. This varies nonlinearly with excitation wavelength and a graphical illustration of the data is given in Fig. 2. It is recalled that in glasses of various compositions this shift of the broadband peak is linear in the energy of the exciting radiation.[14,15]

The fluorescence lifetime of broadband emission was found to fit a single exponential for both materials, the time constants being 10.6 μs for SGGO and 9.9 μs for CGGO. As reported previously,[5] the decay of the R lines is nonexponential when excited in the ${}^4A_2 \rightarrow {}^4T_2$ absorption band. Single exponential decays were obtained by exciting the ${}^4A_2 \rightarrow {}^2E$ transition while detecting only resonantly emitted fluorescence. However, the fluorescence lifetime varied dramatically with wavelength across the line, from 550 to 850 μs in SGGO and from 350 to 450 μs in CGGO, in both cases shortening with increasing wavelength, as is shown in Fig. 3.

In very few crystals [e.g., MgO (Ref. 3)] is the local

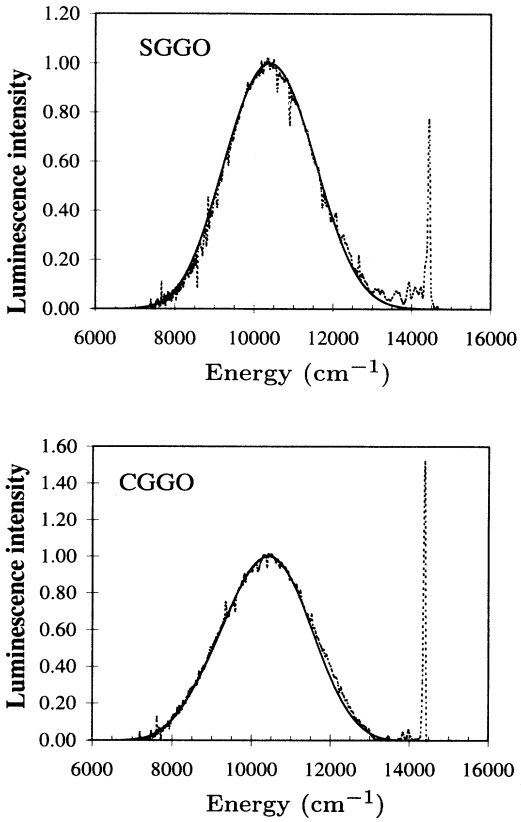

FIG. 1. The fluorescence spectra of SGGO:Cr^{3+} and CGGO:Cr^{3+} at 15 K, corrected for apparatus response (dashed curves). Excitation is in the center of the $^4A_2 \rightarrow {}^4T_2$ absorption band at 17 240 cm^{-1}. The smooth lines represent the results of calculations described in the text to model the fluorescence spectra of the weak-field sites.

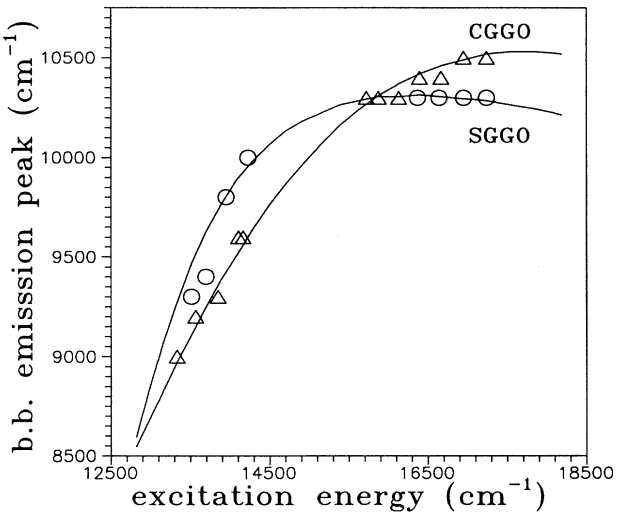

FIG. 2. Dependence of the peak of the broadband emission on excitation energy for SGGO (circles) and CGGO (triangles). The lines represent the results of fitting calculations described in the text.

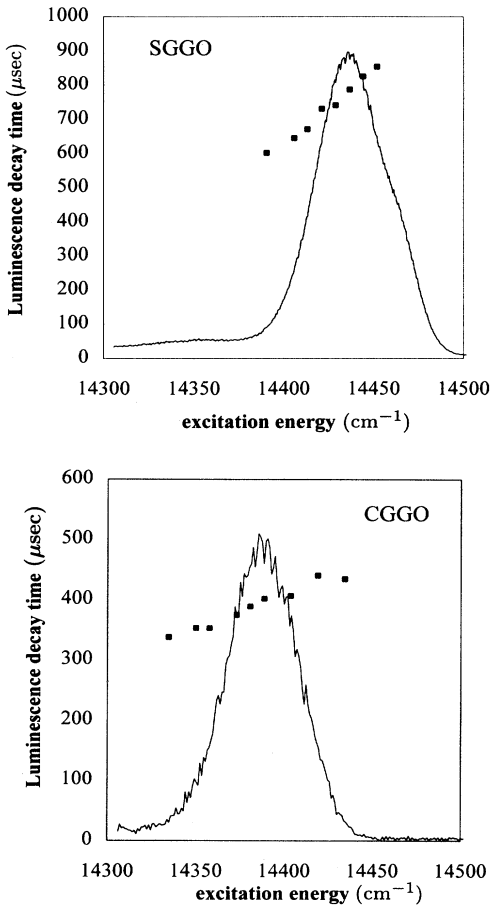

FIG. 3. Dependence of the resonant fluorescence lifetime upon excitation energy for SGGO:Cr^{3+} and CGGO:Cr^{3+} as indicated. The fluorescence line shapes, as excited at 20 000 cm^{-1}, are shown as a guide.

symmetry of the Cr^{3+} ion accurately octahedral such that the $^2E \rightarrow {}^4A_2$ emission is revealed as a single R line. More usually even-parity distortions of the octahedral environment cause splittings of both ^2E and $^4A_2$ states. Generally, the excited-state splitting is much larger than the ground-state splitting,[3] and may sometimes be measured directly in optical spectra as a splitting of the R line. In the case of SGGO (see Fig. 3 and Ref. 5) the splitting of the ^2E state manifests itself as a shoulder on the R line, and a broadening of the R line in CGGO. Little can be deduced as to the origin of these effects without additional information that may be obtained from the FLN data now presented.

Fluorescence line narrowing studies were conducted in two regimes, low and high resolution, in order to separately examine the excited- and ground-state splittings. Spectra obtained using the 1 m monochromator to disperse the fluorescence are shown in Fig. 4 for both host crystals. In this case the resolution of the experimental system is too small to detect the ground-state

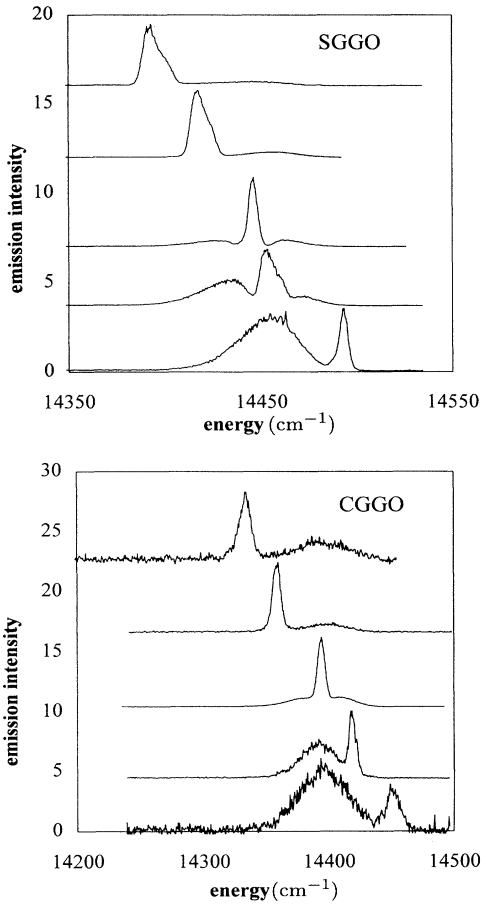

FIG. 4. Fluorescence spectra obtained by resonantly exciting the R lines in SGGO:Cr^{3+} and CGGO:Cr^{3+}, as indicated, and dispersed by the monochromator. Excitation wavelengths are indicated by the peak of the sharpest feature in each spectrum.

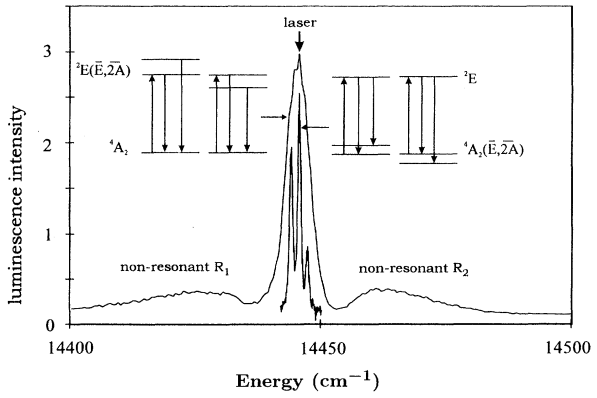

FIG. 5. Comparison of fluorescence line narrowed spectra obtained using the monochromator (outside) and Fabry-Pérot étalon (inside). Arrows indicate the relevant energy levels of Cr^{3+} ions involved in producing each spectrum. See text for fuller expansion.

splitting (Fig. 5). Resonant fluorescence is accompanied by emission that is either red or blue shifted or, in the case of emission excited from the center of the R lines, both. This may be simply explained in terms of the splitting of the excited state into $^2E(\bar{E})$ and $^2E(2\bar{A})$ levels (as the local symmetry is trigonal or pseudotrigonal) so that there are two R-line components, R_1 (lower energy) and R_2. The R_1 line corresponds to the transition from the $\bar{E}$ level which is at lower energy than the $2\bar{A}$ level as the distortion that causes the splitting is a stretch rather than a compression of the octahedron of nearest-neighbor oxygen ions.[3] On the low-energy wing of the composite R line, absorption is exclusively into the R_1 component. Emission is observed resonantly and, after thermalization into the $^2E(2\bar{A})$ state at higher energy, a small amount from the corresponding R_2 line. On the high-energy wing of the composite R line, absorption is exclusively into the R_2 component. Thermalization leads to much of the fluorescence being emitted from the corresponding R_1 state. In between these extremes, absorption may be to either of the two R-line components depending on the crystal field that the absorbing chromium ion experiences. Consequently some ions emit nonresonantly to lower energy and some to higher energy. This explanation is confirmed by repeating the measurements at higher temperatures, resulting in greater thermal occupation of the $^2E(2\bar{A})$ state and a subsequent increase in the strength of the blue-shifted R_2 line emission. Of particular interest to the analysis that follows is the variation in the size of the splitting of the R line as a function of excitation energy, which is interpreted in terms of a variation in the magnitude of the distortion to the octahedral crystal field.

Replacement of the monochromator by a Fabry-Pérot étalon allowed the much smaller $^4A_2$ ground-state splitting to be measured. Again, a three line pattern is obtained (Fig. 5) as a result of the ground-state splitting into two components, $^4A_2(\bar{E})$ and $^4A_2(2\bar{A})$, the explanation in terms of inhomogeneous broadening being entirely analogous to that for the excited state. In Fig. 5 the FLN spectrum excited at the center of the component R line is shown for both low-resolution and high-resolution detection. The three-line pattern due to the ground-state splitting is seen to fit within the resonant line recorded at low resolution where it is therefore not resolved. In the case of the high-resolution spectrum, the free spectral range of the Fabry-Pérot étalon is sufficiently small to cause the fluorescence from nonresonant excited states to appear as a constant background rather than as a specific feature. In ruby, similar three-line patterns corresponding to ground-state splittings have been observed and used to study energy transfer.[16] There was no evidence for energy transfer in gallogermanate hosts; the fluorescence resonant with the laser is the central feature of the three-line pattern in Fig. 5 and the relative line strengths are invariant with delay. The relative intensity of the three ground-state-related fluorescence lines was invariant as a function of excitation wavelength except for the extreme wings of the distribution as expected for a material with large inhomogeneous broadening. The ground-state splitting was also found to be constant for all excitation wave-

lengths to within the limits of experimental resolution, and in agreement with estimated values from EPR spectroscopy.[9]

In summary, the experimental results presented above show that Cr^{3+} ions in SGGO and CGGO occupy two distinct sites which result in different photoluminescence spectra. Those Cr^{3+} ions occupying strong-field sites emit into a strong R-line system with weak vibronic structures whereas weak-field emitters are characterized by a structureless broadband associated with ${}^4T_2 \rightarrow {}^4A_2$ transitions. FLN measurements on the R lines have permitted direct resolution of crystal-field splittings of both ground (${}^4A_2$) and excited (${}^2E$) states of the $3d^3$ ion, demonstrating that the local environments of these Cr^{3+} emitters are distorted from perfectly octahedral symmetry. Excitation spectroscopy and fluorescence decay-time measurements confirm the influence of the crystalline disorder on the material's optical properties. In what follows, the purpose of theoretical analysis is to assess whether disorder influences the octahedral or lower crystal-field splittings and to model the distribution of crystal-field splittings of Cr^{3+} ions in these disordered materials. Finally, such characterizations of the disorder will permit comparison with the mechanisms of disorder known to be present in glasses and other disordered oxides.[6,7,10,11,17,18]

THEORETICAL ANALYSIS

In analyzing the data presented above the approach will be to consider the strong- and weak-field sites independently, assuming that they correspond to the two crystallographically inequivalent sites identified in EPR measurements.[9] Although for higher excitation energies the ratio of the intensity of R-line emission to broadband emission does not depend on excitation wavelength, the decrease in the relative intensity of the R line for excitation energies less than 15 600 cm^{-1} in CGGO,[5] and the large variation in the fluorescence lifetimes between the R lines and the broadband suggest that this approach is justified. This is contrary to the case of another substitutionally disordered material, (Ca,Zr)-substituted $Gd_3Ga_5O_{12}$:Cr^{3+} where spectroscopic data suggest that weak- and strong-field sites are part of the same crystal-field distribution.[17,18]

The ${}^4A_2 \rightarrow {}^4T_2$ absorption transition is a broadband with a maximum at 17 000 cm^{-1} and 16 100 cm^{-1} for SGGO and CGGO, respectively.[5] This is well above the energy of the R-line emission suggesting that this absorption is related to the strong-field sites. However, the excitation spectra of the broadbands are almost identical to the absorption spectra for both materials. Thus, either there is a negligible concentration of weak-field sites, which are excited by nonradiative energy transfer from strong-field sites, or both types of sites have almost identical absorption bands. For both materials, the weak- and strong-field sites are estimated from EPR measurements to be similarly numerous[9] and so the latter assumption is used. The indistinguishable nature of the broad absorption bands from weak- and strong-field sites corresponds to a situation in which the main difference between the sites is in the electron-lattice interaction energy. In the case of weak-field sites the electron-lattice coupling must be sufficiently large that the minimum electronic energy of the ${}^4T_2$ manifold is below the energy of the ${}^2E$ state.

To analyze the spectroscopic data and in particular to reproduce the emission line shapes, we have used an adiabatic model of the electron-phonon interaction in which the first electronic manifold consists of Γ_8 components of the ${}^4T_2$ and the ${}^2E$ states admixed by spin-orbit coupling.[13,19] In this approach the probability of emission from the ith chromium ion is given by

$$P_e(E_1 - E_{\rm em}) \propto \frac{E_{\rm em}^3}{\tau} \left| \int dQ a_{q1}(Q) \chi_1^0(Q) \chi_g^n(Q) \right|^2 , \quad (1)$$

where $\chi_1^0(Q)$ and $\chi_g^n(Q)$ are the vibronic wave functions, Q is the configuration coordinate of the ionic motion, the electronic manifolds being associated with the vibration being denoted by subscripts and the vibronic quantum numbers by superscripts. The ground-state vibronic quantum number n is given by $(E_1^0 - E_g^0 - E_{\rm em})/\hbar\omega$ where $E_{\rm em}$ represents the energy of the emitted photon and $\hbar\omega$ is the energy of the representative phonon. The ${}^4T_2$ state lifetime τ is taken as the fluorescence decay time of the broadband and $a_{ql}(Q)$ is a function which describes the ${}^4T_2$ contribution to the first excited electronic manifold.[13,18]

Distribution of strong-field sites

The low-resolution fluorescence line narrowing results allow the distribution of the energies of the R_1 and R_2 lines to be determined. It is therefore appropriate to begin the analysis of the strong-field sites with a statistical model in which the first moment (most probable value) and standard deviation of the distributions of the density of the ${}^2E(\bar{E})$ and ${}^2E(2\bar{A})$ states are described. Probabilities that the R_1 and R_2 lines have the energy E are given by following convolutions:

$$\Theta_{R_2}(E,\sigma_R) = \int \Theta_2 \left\{ \left[E - \left[E_0 + \frac{\Delta}{2} \right] \right], \sigma_2 \right\} * \Theta_\Delta[(\Delta - \Delta_0), \sigma_\Delta] d\Delta \quad (2a)$$

and

$$\Theta_{R_1}(E,\sigma_R) = \int \Theta_1 \left\{ \left[E - \left[E_0 - \frac{\Delta}{2} \right] \right], \sigma_1 \right\} * \Theta_\Delta[(\Delta - \Delta_0), \sigma_\Delta] d\Delta , \quad (2b)$$

respectively. Here $\Theta_2\{[E-(E_0+\Delta/2)],\sigma_2\}$ and $\Theta_1\{[E-(E_0-\Delta/2)],\sigma_1\}$ describe the distributions of the split components of the ${}^2E$ state around the energies $(E_0+\Delta/2)$ and $(E_0-\Delta/2)$, respectively, whereas $\Theta_\Delta[(\Delta-\Delta_0),\sigma_\Delta]$ is the probability that the splitting is equal to Δ.

This statistical representation is chosen to separate the octahedral and nonoctahedral contributions to the crystal

field. Accordingly, Θ_1 and Θ_2 represent the distribution of the octahedral crystal field whereas the distribution Θ_Δ is related to the distribution of the trigonal component of the crystal field. In general, the distributions of the density of the $^2E(\bar{E})$ and $^2E(2\bar{A})$ states, described by distributions Θ_{R_1} and Θ_{R_2}, and also Θ_1 and Θ_2, are not necessarily equal to each other, especially when some specific relationship between Θ_1, Θ_2, and Θ_Δ is introduced. However, since the splitting Δ should not depend on the octahedral crystal field, we have assumed that the distributions Θ_1 and Θ_Δ, and Θ_2 and Θ_Δ are independent of each other. Under this condition, the standard deviations of the distributions, σ_Δ, σ_1, σ_2, and σ_R are related to each other by Pythagoras' equation. Assuming that $\sigma_1=\sigma_2=\sigma_E$, one obtains

$$\sigma_R=\sqrt{\sigma_E^2+(1/4)\sigma_\Delta^2} \tag{3}$$

for both R_2 and R_1 lines. It should be noted here that the relationship, $\sigma_1=\sigma_2=\sigma_E$, implies that $\Theta_1(E)=\Theta_2(E')$ under the condition that $E'=E+\Delta$. Thus one can use one distribution function Θ_E to represent Θ_1 or Θ_2 when the most probable value of energy is equal to $E_0+\Delta/2$ or $E_0-\Delta/2$, respectively.

The experimental data provide information on the separation between the $^2E(\bar{E})$ and $^2E(2\bar{A})$ states and so it is necessary to relate the statistical model to the probability that when exciting the $^2E(2\bar{A})$ state at energy E the accompanying $^2E(\bar{E})$ state has the energy $E'=E-\Delta$. This probability is denoted as $\Theta_{R_1R_2}(E'=E-\Delta,\Delta_{\text{eff}},\sigma_{\Delta_{\text{eff}}})$, and is equal to the products of the probabilities of the energy splitting being equal to Δ and the average energy of the ^2E states being $(E+E')/2$, once again separating the nonoctahedral and octahedral contributions to the probability distribution. The distribution is characterized by the most probable splitting Δ_{eff}, and the half width of the nonresonant band which is related to the standard deviation of the distribution, $\sigma_{\Delta_{\text{eff}}}$

$$\Theta_{R_1R_2}(E'=E-\Delta,\Delta_{\text{eff}},\sigma_{\Delta_{\text{eff}}})=\Theta_E\left\{\left[E-\left[E_0+\frac{\Delta}{2}\right]\right],\sigma_E\right\}\Theta_\Delta[(\Delta-\Delta_0),\sigma_\Delta]\,. \tag{4a}$$

Similarly, the probability that the upper component of the ^2E state $(2\bar{A})$ has energy Δ greater than E, for the case that excitation is via the R_1 line is given by

$$\Theta_{R_2R_1}(E'=E+\Delta,\Delta_{\text{eff}},\sigma_{\Delta_{\text{eff}}})=\Theta_E\left\{\left[E-\left[E_0-\frac{\Delta}{2}\right]\right],\sigma_E\right\}\Theta_\Delta[(\Delta-\Delta_0),\sigma_\Delta]\,. \tag{4b}$$

Formulas (4) describe the density of nonresonant ^2E components for the resonantly excited multisite system. Occupation of the nonresonant ^2E components is determined by the temperature according to the Maxwell-Boltzmann distribution. When the density of states distributions, $\Theta_{R_1R_2}$ and $\Theta_{R_2R_1}$, are broad this will tend to skew the higher-energy nonresonant line to lower energy and the lower-energy nonresonant line to higher energy. This is because the thermal occupation of strongly split R lines will be more uneven than for R line pairs with small splittings. In this analysis, the shape of the nonresonant lines is irrelevant and the small shift in the measured value of the peak R-line splittings are negligible.

The model developed so far is valid for arbitrary distributions. There are no general statements to relate the peak energies and standard deviations of the distributions $\Theta_{R_1R_2}$ and $\Theta_{R_2R_1}$ to parameters of the distributions Θ_Δ and Θ_E. Relationships can only be obtained for particular distributions. For the purpose of this paper it is useful to assume Gaussian distributions. It is easy to calculate that for all distributions given by Gaussians, the standard deviations of the distributions $\Theta_{R_1R_2}$ and $\Theta_{R_2R_1}$ do not depend on the excitation energy and are equal to

$$\sigma_{\Delta_{\text{eff}}}=2\left[\frac{\sigma_E^2\sigma_\Delta^2}{4\sigma_E^2+\sigma_\Delta^2}\right]^{1/2}, \tag{5}$$

whereas the positions of the maxima of the nonresonant bands depend on the excitation energy, E, as follows:

$$\Delta_{\text{eff}}(R_1R_2)=2(E-E_0)*Q_\Delta+\Delta_0*Q_E\,, \tag{6a}$$

$$\Delta_{\text{eff}}(R_2R_1)=2(E_0-E)*Q_\Delta+\Delta_0*Q_E\,, \tag{6b}$$

where

$$Q_\Delta=\frac{\sigma_\Delta^2}{(\sigma_\Delta^2+4\sigma_E^2)} \tag{7a}$$

and

$$Q_E=\frac{4\sigma_E^2}{(4\sigma_E^2+\sigma_\Delta^2)} \tag{7b}$$

and σ_R, σ_E, and σ_Δ are standard deviations of the respective distributions. Consequently, Δ_{eff} can vary across a broad range of energy depending on the energy of excitation.

The magnitudes of the basic parameters that quantify the statistical model can now be estimated. Assuming that the spectra in Fig. 3, measured at low temperature for excitation into the $^4T_2$ band, correspond mainly to luminescence in the R_1 line, estimates can be made of the parameters of the distribution of the R_1 line, Θ_{R_1}, $E_0-\Delta_0/2$ and σ_R. The weak R_2 contribution comes from ions in sites characterized by small Δ splittings. Thus Eq. (3) allows estimates for σ_E and σ_Δ to be related to σ_R. Furthermore, using the series of resonantly excited fluorescence spectra in Fig. 4 estimates are made of Q_Δ and Q_E, using formulas (6). Estimates of σ_E and σ_Δ follow from formulas (5) and (7). Using formulas (6), the values for the most probable splitting Δ_0 and energy E_0 are estimated. Through an analysis of the line shape of the nonresonant band the standard deviation of the $\Theta_{R_1R_2}$ distribution $\sigma_{\Delta_{\text{eff}}}$ can be obtained.

The experimental data and calculated values of the dis-

TABLE I. Measured and calculated distribution parameters for SGGO:Cr^{3+} and CGGO:Cr^{3+}.

	SGGO	CGGO
Experimentally estimated parameters		
R_1 line position $(E_0-\Delta_0/2)$ (cm^{-1})	14436	14388
σ_R (cm^{-1})	19.4	20.7
$\sigma_{\Delta_{eff}}$ (cm^{-1})	15.9	20.5
Q_Δ	0.21	0.34
Q_E	0.79	0.66
Calculated parameters (cm^{-1})		
σ_E From Eqs. (5) and (7)	17.3	17.5
σ_E From Eq. (3)	17.2	16.4
σ_Δ	18	25
Δ_0 (the most probable value of splitting)	30	22
E_0 (average energy of the ^2E state)	14455	14399

tribution parameters are listed in Table I. The values of σ_R, $\sigma_{\Delta_{eff}}$, and Q_Δ are estimated directly from the experimental results giving three independent equations with only two unknown variables, σ_Δ and σ_E. Thus, one of the unknown quantities σ_E can be obtained in two independent ways. The resulting estimates for σ_E, listed in Table I and corresponding to results from formulas (5) and (7) and then (3), are very similar, suggesting that the statistical model is reliable.

The results of this analysis confirm the considerable extent of the inhomogeneous broadening of the R_1 and R_2 lines in chromium-doped gallogermanates arising from the broad distribution of the crystal field at the chromium sites. Although there is no correlation between the magnitude of the ^2E splitting and the octahedral component of the crystal field, there is a correlation between the energies of the two components of the ^2E level and the splitting between them, Δ. This results from the large distribution of the R-line splitting. The R line is split symmetrically with respect to E_0 when there is no contribution to the inhomogeneous broadening from the octahedral crystal field. However, this is not the case. The resulting intensities of the nonresonant bands are therefore given by the distributions in Eqs. (4). The experimentally determined dependence of the position of the nonresonant bands on the excitation energy is presented in Fig. 6. The statistical model yields a linear dependence of the energies of the nonresonant bands on the excitation energy and reproduces the experimental data. Nevertheless, in both CGGO and SGGO, the half width of the octahedral field distribution is smaller than the half width of the distribution of the splitting energy, meaning that the principal inhomogeneous broadening mechanism for the R lines is the distribution of the trigonal component of the crystal field. Thus the disorder in gallogermanates is related to those defects which break the octahedral symmetry at the Cr^{3+} sites, rather than to changes of the lattice constant or the size of the octahedron of nearest-neighbor oxygen ions which influence the $10Dq$ parameter.

The statistical model also explains the shapes of the R-line luminescence spectra that result from excitation into the $^4T_2$ band (Fig. 3). A shoulder represents the contribution of the R_2 line in the case of SGGO but there appears to be no contribution from the R_2 line for CGGO. The results in Table I show that the standard deviation of the distribution of the splitting energy σ_Δ is considerably greater than the most probable splitting Δ_0 in CGGO but not in SGGO. In consequence, the inhomogeneous broadening almost completely mixes the R_1 and R_2 lines in CGGO but less strongly in SGGO. This result shows that the disorder is stronger in CGGO (in which σ_Δ is larger) whereas the distortion is stronger in SGGO (in which Δ_0 is larger).

The relationship between the fluorescence decay time and excitation energy in Fig. 3 can also be explained using the statistical model. Since the correlation between the absolute energy of the R_1 line and the size of splitting is significant, the changes in luminescence decay time may be attributed to the influence of the trigonal distortion of the field rather than to the strength of the octahe-

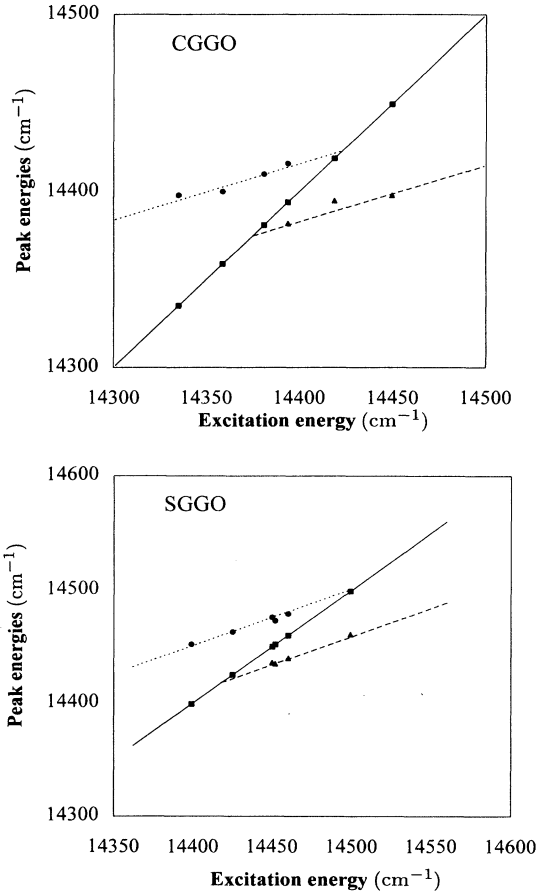

FIG. 6. Plots of resonant and nonresonant feature energies corresponding to excited state splittings of R lines in CGGO:Cr^{3+} and SGGO:Cr^{3+} as indicated. Squares represent resonant features, circles nonresonant emission from R_2 levels and triangles nonresonant emission from R_1 levels.

dral crystal field. It is reasonable to assume that fluorescence in the R_1 line dominates at low temperatures and so, as the excitation energy is increased, states characterized by increasingly small splittings are excited.

To account for the R-line lifetime data it is necessary to consider the interaction of the electrons in the $^4T_2$ state with the crystal field. This interaction should be much greater than in the ^2E state and will dominate the determination of the $^2E \rightarrow {}^4A_2$ transition probability. The octahedral and nonoctahedral components are considered separately.

(1) The octahedral crystal field. The electron-lattice coupling energy remains constant ($S\hbar\omega = 1900$ cm^{-1}) and so the mixing of the $^4T_2$ wave function into the ^2E wave function will vary almost linearly with the separation between the energy minima of the states. The configuration coordinate diagram for this case is shown in Fig. 7, marked 1.

(2) The distortion to the octahedral crystal field. Coupling to nonsymmetric vibrational modes can result in an increase in the effective electron-phonon coupling strength in the $^4T_2$ state, reducing the minimum energy of the manifold. This effect (related to the Jahn-Teller effect) will be stronger for more distorted sites with larger ^2E splittings corresponding to low-energy resonant excitation. It should be noted that such an effect will not change the octahedral crystal-field component when the average distance between the central ion and the ligands remains fixed. The admixture of the states is no longer linear with energy separation. The configuration coordinate diagram for this case is shown in Fig. 7, marked 2.

The radiative transition probabilities have been calculated for both of these two cases using the adiabatic model[13] and the resulting lifetimes are plotted in Fig. 8. For case 2, when resonantly exciting to the ^2E state, the crossing points of the energies of the $^4T_2$ electronic manifolds of all sites correspond to the configuration coordinate where the ^2E electronic manifold has a minimum and so the energy of the $^4T_2$ electronic manifold is the same for each site. This case corresponds to constant octahedral crystal field. Sites with lower $^4T_2$ energy minima have stronger electron-lattice coupling as the value of $S\hbar\omega$ follows the energy of the $^4T_2$ state thus varying from 1650 to 2150 cm^{-1} and from 970 to 1230 cm^{-1} at the half width of the distributions of SGGO and CGGO, respectively. As a result of this, changes in the radiative transition probability are much lower than for case 1. Intermediate cases, for which both octahedral crystal field and electron-phonon coupling vary, yield results that produce dependencies between those of curves 1 and 2 in Fig. 8. The analysis of the FLN data above has shown that the nonoctahedral component of the crystal field dominates the inhomogeneous broadening of the R lines in gallogermanates. It is therefore assumed that curve 2 provides a more realistic relationship, in particular for SGGO, and this is used for subsequent calculations of strong-field site distribution parameters.

The fluorescence lifetimes at the half-width energies of the R_1 line can be obtained from Fig. 3. From Fig. 8 the $^2E - {}^4T_2$ energy separation can be obtained for these lifetimes and this must correspond to the half width of the distribution of $^2E - {}^4T_2$ energy separations. It then becomes possible to build a complete model of the distribution of strong-field sites. Representative configuration

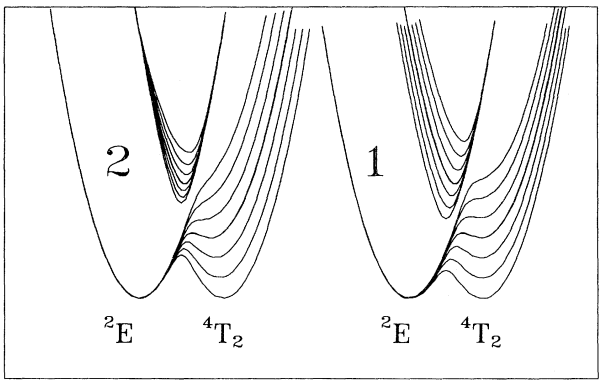

FIG. 7. Representative excited-state configuration coordinate diagrams for strong-field sites corresponding to models 1 and 2, discussed in the text.

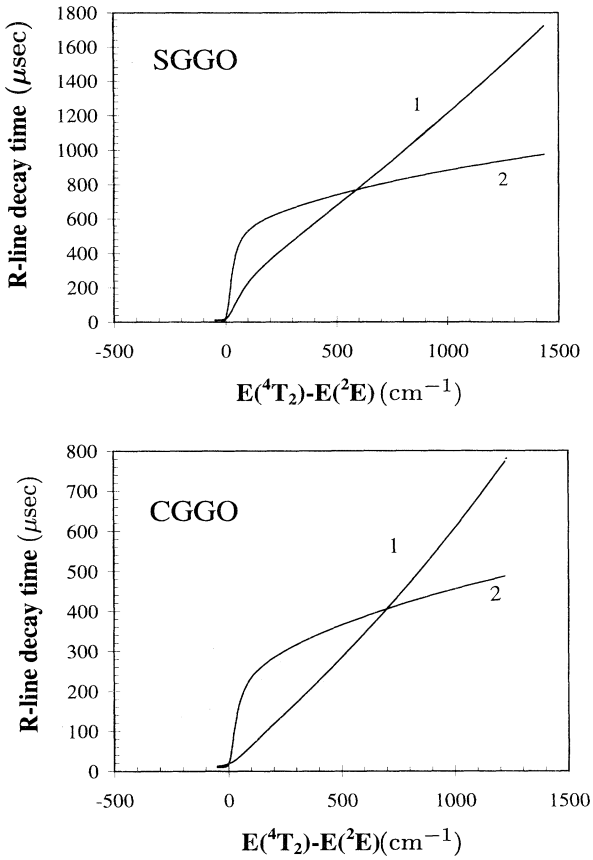

FIG. 8. Fluorescence lifetimes for strong-field sites as calculated from models 1 and 2, discussed in the text, plotted as a function of the separation of the ^2E and $^4T_2$ states for SGGO:Cr^{3+} and CGGO:Cr^{3+} as indicated.

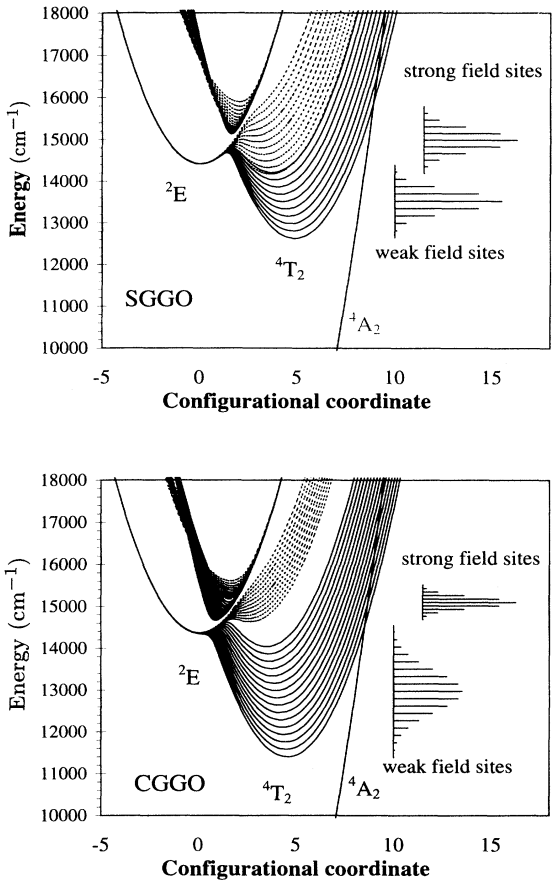

FIG. 9. For SGGO:Cr^{3+} and CGGO:Cr^{3+}, as indicated, representative configuration coordinate diagrams for the multisite system (left) and the density of states corresponding to each $^4T_2$ minimum (right), calculated as described in the text. Strong-field sites are indicated by dotted lines and weak-field sites by solid lines. The configuration coordinate in this figure is an effective coordinate that is chosen, in many-dimensional configuration coordinate space to connect the points where the ^2E and $^4T_2$ electronic manifolds have minimum energy. The units of the configuration coordinate are $(\hbar/M\omega)^{1/2}$ where M is the effective ionic mass of the vibrating ions.

coordinate diagrams are shown with dotted lines in Fig. 9 together with histograms that represent the distribution. The configuration coordinate parameters are given in Table II and obtained assuming that the absorption characteristics of the strong-field sites are similar to those of the weak-field sites discussed below. It can be seen the distribution of strong-field sites leads to some ions with $^2E-{}^4T_2$ energy separations that are close to or less than zero. Figure 8 shows that the fluorescence lifetime for such centers should be much smaller than that measured. However, this behavior is only to be expected on the wings of the R lines where signal strength prevented lifetime measurements from being performed. The fluorescence lifetime and FLN data are therefore both consistent with the configuration coordinate diagrams produced from the model.

A consideration that has not been taken account of so far is the odd-parity crystal-field contribution of the distortion Hamiltonian. This does not cause the splitting of the R lines but will increase the electric dipole transition probability. If the odd-parity lattice distortion has a similar distribution to the nonoctahedral component of the crystal field the variation in fluorescence lifetime could be partially accounted for in this way. However, EPR results suggest that the main distortion to the oxygen octahedra is a stretch along the c axis, an even-parity perturbation, and it is therefore unlikely that the contribution of odd-parity distortion induced electric dipole transitions is significant. The fluorescence lifetime data can be well reproduced without considering the odd-parity distortion and so it is considered to be negligible.

There are strong arguments which support the notion that the optical properties of gallogermanates result principally from the low-symmetry crystal-field contribution. Previous studies of Cr^{3+}-doped lattices have shown that when the octahedral crystal field increases, the energy of the ^2E state usually decreases. This effect has been confirmed by high-pressure spectroscopy of ruby,[20,21] alexandrite,[22] elpasolite,[23] and garnets[24] where increases in the R-line decay times are usually accompanied by a decrease in the ^2E energy. Thus, if changes in R-line decay times are related only to changes of the effective octahedral crystal field, it would be expected that the shortest decays should be observed on the higher-energy side of the R line contrary to the experimental results for gallogermanates. It is therefore concluded that model 2, which predicts that the minimum energy of the $^4T_2$ electronic manifold is decreased mainly by the electron-lattice interaction, is realistic.

Distribution of weak-field sites

Assuming that the distribution of the energies of the $^4T_2$ states is broad, the line shape of the absorption spectrum of the multisite system, $I_{ex}(E_{ex},\sigma_{ex})$, can be calculated as follows:

$$I_{ex}(E_{ex},\sigma_{ex})=\sum_i P_a(E_{ex}-E_i,\sigma_i)\Theta_a(E_i,\sigma_a,\sigma_i)\ , \tag{8}$$

where E_{ex} is the excitation energy and E_i is defined as the minimum energy of the $^4T_2$ electronic manifold of the ith site. The functions $P_a(E_{ex}-E_i,\sigma_i)$ and $\Theta_a(E_i,\sigma_a,\sigma_i)$ are, respectively, the probability of absorption and the site distribution relating to absorption at this energy. The quantity σ_i is the standard deviation of the absorption band of the ith site and σ_a is the standard deviation of the distribution Θ_a. For a Pekarian absorption line shape[3]

$$\sigma_i=\sqrt{S_i}\hbar\omega\ , \tag{9}$$

where S_i is Huang-Rhys factor for the ith site. The quantity Θ_a depends on the energy of the $^4T_2$ electronic manifold for ions occupying the equilibrium position of the ground state $^4A_2$ electronic manifold. Thus Θ_a also depends on σ_i.

The standard deviation of the convolution given in Eq.

TABLE II. Configuration coordinate diagram parameters for Cr^{3+} in SGGO and CGGO (wave numbers). Spin-orbit parameter $\xi=210\ cm^{-1}$, $\hbar\omega=250\ cm^{-1}$.

	Mean electron lattice coupling energy ($S\hbar\omega$)	Standard deviation of $S\hbar\omega$ distribution	Mean $^4T_2-{}^2E$ energy	Standard deviation of $^4T_2-{}^2E$ energy	K
		Strong-field sites			
SGGO	1900	250	550	250	1.0
CGGO	1100	130	700	130	1.0
		Weak-field sites			
SGGO	3700	320	−900	250	1.3
CGGO	3200	330	−1400	500	0.65
		Energy distribution			
		Maximum	Standard deviation		
SGGO					
Θ_e		9900	570		
Θ_a		17000	80		
CGGO					
Θ_e		9900	830		
Θ_a		16000	180		

(8), σ_{ex}, is greater than the standard deviation of the absorption and the standard deviation of the site distribution. When electron-lattice coupling is the same for each site $\sigma_i=\sigma$, one obtains, from the Pythagoras relationship

$$\sigma_{ex}=\sqrt{(\sigma^2+\sigma_a^2)}\ . \tag{10}$$

The emission line shape I_{em} also depends on the excitation energy E_{ex} and the excitation conditions. The experimental conditions under which spectra were obtained here can be considered to be those of weak excitation in that the average period an optically active ion spends in the ground state between excitations is large compared to the fluorescence lifetimes. Then the intensity of the emission is dependent only on the intensity of exciting light and the absorption cross section of the material. In order that the expression for emission intensity is independent of fluorescence lifetime, which is very different for strong- and weak-field sites, a normalized relative emission probability, $P_e(E_i-E_{em},\sigma_i)$, is introduced and results in the following expression:

$$I_{em}(E_{em},\sigma_{em},E_{ex})=\sum_{i}^{E_i<E_{ex}} P_a(E_{ex}-E_i,\sigma_i) * \Theta_c(E_i,\sigma_e,\sigma_i) \times P_e(E_i-E_{em},\sigma_i) \tag{11}$$

for monochromatic excitation. The summation is for those sites for which the energy of the minimum of the $^4T_2$ electronic manifold is lower than E_{ex}. For any given excitation energy, an effective site distribution can be defined

$$\Theta'_e(E_i,E_{ex},\sigma'_e)=P_a(E_{ex}-E_i,\sigma_i)\Theta_e(E_i,\sigma_e,\sigma_i)\ , \tag{12}$$

which corresponds to the probability of a chromium ion in the ith site being excited by energy E_{ex}.

It has already been assumed that σ_i appears as an additional parameter in the site distribution functions, Θ_a and Θ_e. If the site distribution is such that both E_i and the value of the electron-lattice coupling, represented by the Huang-Rhys factors S_i, are variables then the expressions for emission and absorption are given by

$$\Theta_e(E_i,\sigma_e,\sigma_i)=\Theta_e(E_i-S_i\hbar\omega,\sigma_e) \tag{13a}$$

and

$$\Theta_a(E_i,\sigma_a,\sigma_i)=\Theta_a(E_i+S_i\hbar\omega,\sigma_a)\ , \tag{13b}$$

respectively, where $\hbar\omega$ is the characteristic phonon energy. It is useful to note at this point that the octahedral distribution of the crystal field is described by Θ_a.

In the simplest case, the Huang-Rhys factor is approximated as being the same for all sites so that the site distributions for absorption and emission are independent of σ_i and equal to each other:

$$\Theta_a(E_i,\sigma_a)=\Theta_e(E_i,\sigma_e)=\Theta(E_i,\sigma_\Theta)\ . \tag{14a}$$

Then

$$\sigma'_e=\frac{\sigma_e\sigma_\Theta}{\sqrt{\sigma_e^2+\sigma_\Theta^2}}\ . \tag{14b}$$

This is the expected behavior when the sites differ only by the strength of the octahedral crystal field.

Equations (12) and (14) imply that a broad site distribution should result in the standard deviation of the emission spectrum being smaller than the standard deviation of the absorption spectrum. However, the experimental spectra show the opposite behavior. This phenomenon can be explained by assuming that the site distribution for emission Θ_e is much broader than the respective site

distribution for absorption Θ_a.

Use of the relationships (13) correspond to the Huang-Rhys factor increasing as the energy of the $^4T_2$ state decreases. It has been shown that almost all of the decrease in energy of the $^4T_2$ state is caused by electron-lattice interaction. This means that the quantity $E_i+S_i\hbar\omega$ has almost the same value for each site, whereas $E_i-S_i\hbar\omega$ varies at twice the rate of E_i, resulting in a very narrow site distribution for absorption and a very broad site distribution for emission. As discussed above for the strong-field sites, this corresponds to the case where the site distribution is related to the distribution of lower symmetry crystal-field contributions rather than to the distribution of the octahedral crystal-field characterizing parameter $10Dq$.

The basic parameters of the site distribution, σ_a and σ_e, can be estimated by considering the dependence of the broadband luminescence maximum on the energy of excitation. For this purpose, calculations have been performed to simulate the emission spectra using formula (11). In defining the site distribution it has been assumed that the Huang-Rhys parameter changes linearly with energy E_i. Thus, for the ith site,

$$S_i\hbar\omega=S_0\hbar\omega-K(E_i-E_0)\ , \tag{15}$$

where E_0 and S_0 are defined as being the most probable value of the minimum energy of the $^4T_2$ manifold and the most probable value of the Huang-Rhys factor, respectively. Gaussian shapes are assumed for both site distributions. The parameter K is a constant, the value of which describes to some extent the influence of the lower-symmetry field. When $K=0$, all variation in the crystal field is due to the octahedral contribution whereas when $K=1$ the crystal field variation is due exclusively to the nonoctahedral distortion. All other cases, $0<K<1$ and $K>1$, correspond to situations where there is variation in both symmetries. Equations (13) and (15) allow the standard deviations of the site distributions adequate for calculation of the absorption and emission bands to be defined as follows:

$$\sigma_a=|(1-K)|\sigma_\Theta\ , \tag{16a}$$

$$\sigma_e=(1+K)\sigma_\Theta\ , \tag{16b}$$

where σ_Θ is the standard deviation of the distribution of the energy of the minimum of the $^4T_2$ electronic manifold. From Eq. (16) it follows that the standard deviation of the distribution of the Huang-Rhys factor is given by $\sigma_s=K\sigma_\Theta$. The probability of $^4A_2\rightarrow{}^4T_2$ absorption, $P_a(E_{ex}-E_i,\sigma_i)$, was calculated using the standard Pekarian form

$$P_a[E_{ex}-E_i,\sigma_i(S_i)]=\frac{e^{-S_i}S_i^n}{n!}\delta[E_{ex}-(E_i+n\hbar\omega)]\ . \tag{17}$$

Since a very broad distribution of the energies of the $^4T_2$ state is expected there is a possibility that for some sites the energy separation from the ^2E doublet is very small or even zero. This is one reason why the emission spectra have been modeled using the adiabatic model and calculated using formula (1).

Using this model, the dependence of the energy of the broadband peak on the excitation energy has been calculated (Fig. 2). It is assumed that the absorption maximum corresponds to the maximum of the distribution Θ_a, and the parameters of the weak-field distribution (i.e., the most probable energy of the $^4T_2$ electronic manifold, the expected electron-lattice interaction energy, $S\hbar\omega$, and their standard deviations) have bene treated as free parameters. The decrease in the emission peak at very high excitation photon energies is caused by rounding errors. In Fig. 9 the configuration coordinate diagrams of the weak-field sites are shown together with histograms representing the best-fit distributions. Knowing the distribution of the weak-field sites it was possible to reproduce the broadband fluorescence line shape shown in Fig. 1 where it is compared with the measured spectrum.

The parameters for the configuration coordinate diagrams are listed in Table II. The distribution of the weak-field sites is very broad in both materials. The standard deviation of the distribution of the electron-lattice interaction energy σ_s is similar for both hosts at 325 and 320 cm^{-1} for CGGO and SGGO, respectively. However, the site distribution is additionally broadened in CGGO by the distribution of the average octahedral field, which is almost negligible in SGGO.

There is strong evidence for the dominating influence of the distribution of nonoctahedral crystal-field components in the weak-field sites. For instance, the emission spectrum is broadened, as a result of the distribution of the electron-lattice interaction energy, to the extent that it is as broad as the absorption spectrum. Furthermore, the maximum energy of broadband emission should vary linearly with excitation energy when the sites differ by only the $10Dq$ parameter, as is the case in glasses of various chemical compositions.[13,14] This is not the case for either SGGO or CGGO though the plot of peak emission against excitation energy is more linear over a broader range for CGGO than SGGO due to the greater influence of octahedral inhomogeneity in the former. As for the strong-field sites, it has been shown that the inhomogeneous broadening of the weak-field sites is dominated by nonoctahedral contributions to the crystal field and that the smaller contribution of the octahedral crystal field is more pronounced in CGGO than in SGGO.

CONCLUSIONS

The inhomogeneous broadening of optical transitions of impurities in solids is usually caused by variations in the local crystal field experienced by the optically active ion. It is frequently sufficient to consider only variations in the strength of the crystal field to account for both the broadening of the transition and the variation of attendant characteristics of optical behavior that may be measured through selective excitation.

It is usual for the configuration of Cr^{3+} nearest neighbors in oxides to be an approximate octahedron of oxygen ions.[3] Variation in the size of the octahedra causes large variations in the strength of the crystal field resulting in broadened transitions. This has been observed, for instance, in silicate and Li borate glasses where the R lines are broadened to about 200 cm^{-1}. This broadening

was confirmed to be due to variations in the strength of the octahedral field using FLN Zeeman spectroscopy.[7]

When the host lattice is crystalline the magnitude of inhomogeneous broadening is expected to be much smaller, reflecting the order of the crystal field. However, when the host crystal contains sites that may be occupied randomly by two or more constituent ions, substitutional disorder may cause a number of crystallographically equivalent centers to be spectroscopically distinguished. For instance, five $^2E \rightarrow {}^4A_2$ transitions due to nonequivalent Cr^{3+} centers have been observed in yttrium aluminum garnet and attributed to different configurations of second-nearest neighbors that alter the size of the oxygen octahedra.[8] Nevertheless, the inhomogeneous broadening of each of these lines may be attributed to variation of the octahedral field at the Cr^{3+} ion. Alternatively, the individual environments that result from the random occupation of second-nearest neighbors may be such that all contributions to the fluorescence spectrum appear to produce a single, very broad line. This is the case in $CaYAlO_4$ in which the single R line is broadened to greater than 100 cm^{-1}.[25]

A further complication in the broadening of Cr^{3+} optical transitions is the splitting of the energy levels caused by distortions of the oxygen octahedra. The splittings that result from such reductions in the symmetry of the crystal field at the Cr^{3+} ion have been discussed above. Again, the octahedral component of the crystal field usually dominates the inhomogeneous broadening of resulting spectral features, the splitting due to the crystal field being almost constant for all ions.

This study of Cr^{3+} impurities in gallogermate hosts has shown the existence of a new mechanism for inhomogeneous broadening. While there is a contribution to the inhomogeneous broadening of both the R-line and broadband fluorescence from the purely octahedral component of the crystal field, the observed behavior is dominated by variation in the size of distortions to the oxygen octahedra. In the case of the strong-field sites this manifests itself experimentally as a variation in the separation between resonant and nonresonant components of FLN spectra and as a variation of the fluorescence lifetime as a function of excitation energy. Such is the extent of this effect that the R-line fluorescence appears as a single line despite large splittings of the energy levels of the individual Cr^{3+} ions. For weak-field sites, it is the large variation in the coupling to nonsymmetric vibrational modes that results in a strong dependence of the peak fluorescence energy on excitation energy and in a broadened fluorescence spectrum.

It is reasonable to expect that the defects responsible for broad energy distributions in both weak- and strong-field sites have a common cause. The distribution of distortions from octahedral symmetry has been shown to dominate the contribution of the distribution of octahedral crystal fields for both sets of sites. It is also reasonable to expect that the source of this disorder is the random statistical occupation of $Ga^{3+}$and Ge^{4+} sites that influence the precise size and shapes of nearby oxygen octahedra, resulting in a large number of environments for the Cr^{3+} ions. It would then have to be assumed that the crystal field experienced by the Cr^{3+} ions divides into two distributions, each causing either the ^2E or the $^4T_2$ level to be at slightly higher energy than the other. Further information on the precise nature of the sites may be gained from EPR measurements.[9]

The identification of a new mechanism for inhomogeneous broadening has important implications for laser gain media. In order to produce materials capable of providing optical gain over large wavelength ranges for utilization in tunable or ultrashort pulse lasers it is necessary to maximize the width of the emission bands. An understanding of the physical principles underlying the nature of broadening mechanisms is essential to fully understand the operational characteristics of devices, for the identification of potential new materials, and for the general development of crystal-field engineering.

ACKNOWLEDGMENTS

The authors wish to thank Professor Mitsuo Yamaga of Gifu University, Japan and Dr. H. Takeuchi of Nagoya University, Japan for a preview of their EPR measurements and for useful discussions of this work. K.H. thanks the Nuffield Foundation for partial support of his work and P.M. thanks DRA Malvern and EPSRC for financial support of his study. Travel and accommodation grants from the Royal Society, The British Council, and Komitet Badan Naukowych are also gratefully acknowledged.

[1]L. Zhang, J. Yu, and S. Huang, J. Lumin. **45**, 301 (1989).
[2]K. Holliday, C. Wei, M. Croci, and U. P. Wild, J. Lumin. **53**, 227 (1992).
[3]B. Henderson and G. F. Imbusch, *Optical Spectroscopy of Inorganic Solids* (Oxford University Press, Oxford, 1989).
[4]B. Struve, G. Huber, V. V. Laptov, I. A. Schcherbakov, and E. V. Zharikov, Appl. Phys. B **30**, 117 (1983).
[5]P. I. Macfarlane, T. P. J. Han, B. Henderson, and A. A. Kaminskii, Opt. Mater. **3**, 15 (1994).
[6]F. Bergin, J. F. Donegan, T. J. Glynn, and G. F. Imbusch, J. Lumin. **34**, 307 (1986).
[7]C. Ogihara, Y. Gao, K. P. O'Donnell, B. Henderosn, and M. Yamaga, J. Phys. Condens. Matter **4**, 8151 (1992).
[8]W. Nie, G. Boulon, and J. Mares, Chem. Phys. Lett. **160**, 597 (1989).
[9]M. Yamaga and H. Takeuchi (private communication).
[10]C. J. Donnelly, S. H. Healy, T. J. Glynn, G. F. Imbusch, and G. P. Morgan, J. Lumin. **42**, 117 (1988).
[11]M. Yamaga, K. P. O'Donnell, Y. Gao, and B. Henderson, Appl. Phys. B **51**, 132 (1990), and references therein.
[12]A. A. Kaminskii, A. V. Butashin, A. A. Demidovich, V. G. Kotev, B. V. Mill, and A. P. Shkadarevich, Phys. Status Soli-

di A **112**, 197 (1989).
[13]M. Grinberg, J. Lumin **54**, 369 (1993).
[14]M. Yamaga, B. Henderson, K. P. O'Donnell, and Y. Gao, Phys. Rev. B **44**, 4853 (1991).
[15]B. Henderson, M. Yamaga, Y. Gao, and K. P. O'Donnell, Phys. Rev. B **46**, 652 (1992).
[16]P. M. Selzer, D. L. Huber, B. B. Barnett, and W. M. Yen, Phys. Rev. B **17**, 4979 (1978).
[17]A. Brenier, G. Boulon, C. Pedrini, and C. Madej, J. Appl. Phys. **71**, 6062 (1992).
[18]M. Grinberg, A. Brenier, G. Boulon, C. Pedrini, and C. Madej, J. Lumin. **55**, 303 (1993).
[19]M. Yamaga, B. Henderson, and K. P. O'Donnell, Phys. Rev. B **46**, 3273 (1992).
[20]G. J. Piermarini, S. Block, J. D. Barnett, and R. Forman, J. Appl. Phys. **46**, 2274 (1975).
[21]S. M. Sarma and Y. M. Gupta, Phys. Rev. B **40**, 3329 (1989).
[22]T. Kottke and F. Williams, Phys. Rev. B **28**, 1923 (1983).
[23]A. G. Rinzler, J. F. Dolan, L. A. Kappers, D. S. Hamilton, and R. H. Bartram, J. Phys. Chem. Solids **54**, 89 (1993).
[24]D. Galanciak, P. Perlin, M. Grinberg, and A. Suchocki, J. Lumin **60&61**, 223 (1994).
[25]M. Yamaga, H. Takeuchi, K. Holliday, P. I. Macfarlane, and B. Henderson, J. Defect (to be published).